

Journal of Materials Chemistry C

Accepted Manuscript



This is an *Accepted Manuscript*, which has been through the Royal Society of Chemistry peer review process and has been accepted for publication.

Accepted Manuscripts are published online shortly after acceptance, before technical editing, formatting and proof reading. Using this free service, authors can make their results available to the community, in citable form, before we publish the edited article. We will replace this *Accepted Manuscript* with the edited and formatted *Advance Article* as soon as it is available.

You can find more information about *Accepted Manuscripts* in the [Information for Authors](#).

Please note that technical editing may introduce minor changes to the text and/or graphics, which may alter content. The journal's standard [Terms & Conditions](#) and the [Ethical guidelines](#) still apply. In no event shall the Royal Society of Chemistry be held responsible for any errors or omissions in this *Accepted Manuscript* or any consequences arising from the use of any information it contains.



Journal Name

ARTICLE

Self-assisted nucleation and growth of [010]-oriented Sb₂Se₃ whisker: the crystal structure and thermoelectric property

Hsin-jay Wu,^a Ping-chung Lee,^b Fan-yun Chiu,^b Sinn-wen Chen^c and Yang-yuan Chen^b

Received 00th January 20xx,
Accepted 00th January 20xx

DOI: 10.1039/x0xx00000x

www.rsc.org/

The layered-chalcogenide Sb₂Se₃ has potential for use in photovoltaic device and thermoelectric cooler, but the practical applications are restricted as bulk Sb₂Se₃ exhibits high electrical resistivity (ρ). Herein, we synthesize *n*-type Te-doped Sb₂Se₃ whisker with the average feature size of 1cm in length and 200 μ m in width via a self-assisted vapor-solid (VS) method. In particular, based on the crystallographic identification using techniques of Powder X-ray diffraction and Transmission Electron Microscopy, the Te-doped Sb₂Se₃ whisker grows along a preferred orientation of [010], which is rarely reported for an orthorhombic structure that the bonding energy along *c*-axis is much stronger. The [010]-oriented Sb₂Se₃ whisker shows enhanced electrical conductivity, especially comparing with its bulk form, and exhibits high Seebeck value (*S*) within 300K-400K, resulting in a peak power factor (S^2/ρ) of ~ 7.6 (μ W/mK²) at 350K. The peak *PF* value is 10⁴ higher than that of Sb₂Se₃ bulk and is comparable to that of Sb₂Se₃ nanotube, respectively, giving rise to the possibility of utilizing the Sb₂Se₃ in the application of thermoelectric cooler.

1. Introduction

Semiconductor materials with preferred orientations, such as the one-dimensional nanowires or nanotubes¹⁻³, the single crystals showing high anharmonicity⁴, etc., demonstrate distinct electronic and thermal transport properties compared with that of their bulk materials, leading to considerable breakthroughs in various research areas. The Sb₂Se₃, which belongs to the family of layered-chalcogenide V₂VI₃ (V=Sb, Bi; VI=S, Se, Te), adopts a highly anisotropic orthorhombic structure with *Pnma* space group and is being considered as a potential candidate in lots of research fields^{5,6}. In particular, the one-dimensional^{7,8} or thin-film Sb₂Se₃⁹ shows excellent photovoltaic and thermoelectric properties, and has applications in photovoltaic device^{10,11}, in switching memory^{12,13}, in thermoelectric cooler¹⁴ and in thermopower wave sources¹⁵⁻¹⁷ that could possibly generate much more power than that estimated in the classic thermoelectric calculations. This fact motivates the research interest extended from one of the family members, the Bi₂Te₃, which has long been developed in thermoelectric cooler¹⁸ and topological insulator¹⁹, to the comparably less-explored Sb₂Se₃.

Thermoelectric materials attract growing attention due to the capability of turning waste heat into precious electricity, which might be a cure for the worldwide energy crisis²⁰. The efficiency of thermoelectric material is guided by a

dimensionless group, $zT=(S^2/\rho\kappa)T$, where *S* refers to the thermopower ($S=\Delta V/\Delta T$), ρ stands for the electrical resistivity and κ is the thermal conductivity. The worldwide researchers are keen to enhance the term S^2/ρ , which also referring to materials' power factor (*PF*), by pursuing high electrical current and large voltage, and to reduce the thermal conductivity, by increasing the phonon scattering through nanostructuring²¹.

Efforts are underway to develop the Sb₂Se₃ as a promising thermoelectric material, motivated by its extraordinary high *S* of 1800(μ V/K) at room temperature^{22,23}. Nevertheless, bulk Sb₂Se₃ exhibits high ρ of 10²-10⁶(Ω m), degrading its *PF* value²²⁻²⁴ and making it less attractive as a thermoelectric material. Thanks to the development of nanotechnology, the electrical resistivity of one-dimensional sulfurized Sb₂Se₃ nanowires and nanotubes reaches extremely low values of 10⁻³-10⁻⁴ (Ω m) while *S* retains as high as -750(μ V/K)¹⁴, leading to moderate *PF* values of 10⁻³-10⁻⁴ (Wm⁻¹K⁻²) that falls in a similar range compared with that of *n*-type Se-doped Bi₂Te₃ at room temperature²⁵.

As mentioned above, a recently discovered phenomenon, named thermopower wave, serves as an alternative way for generating the electricity from the thermal energy, which is inspired by the Seebeck effect but showing higher output power than that of traditional thermoelectric device¹⁵⁻¹⁷. Utilizing the carbon nanotubes that filled with explosive fuel into an electricity-generating system, for example, demonstrates a tremendous peak power of 7 (kW/kg)¹⁵ as the fuel combusts and the exothermic reaction takes place along the tube, providing huge thermal gradient that could be converted into electricity. Similarly, the layered-chalcogenide Bi₂Te₃ or Sb₂Te₃ holds the potential for application in

^a Department of Materials and Optoelectronic science, National Sun Yat-sen University, Kaohsiung 80424, Taiwan.

^b Institute of Physics, Academia Sinica, Taipei 11529, Taiwan.

^c Department of Chemical Engineering, National Tsing Hua University, Hsinchu 30013, Taiwan.

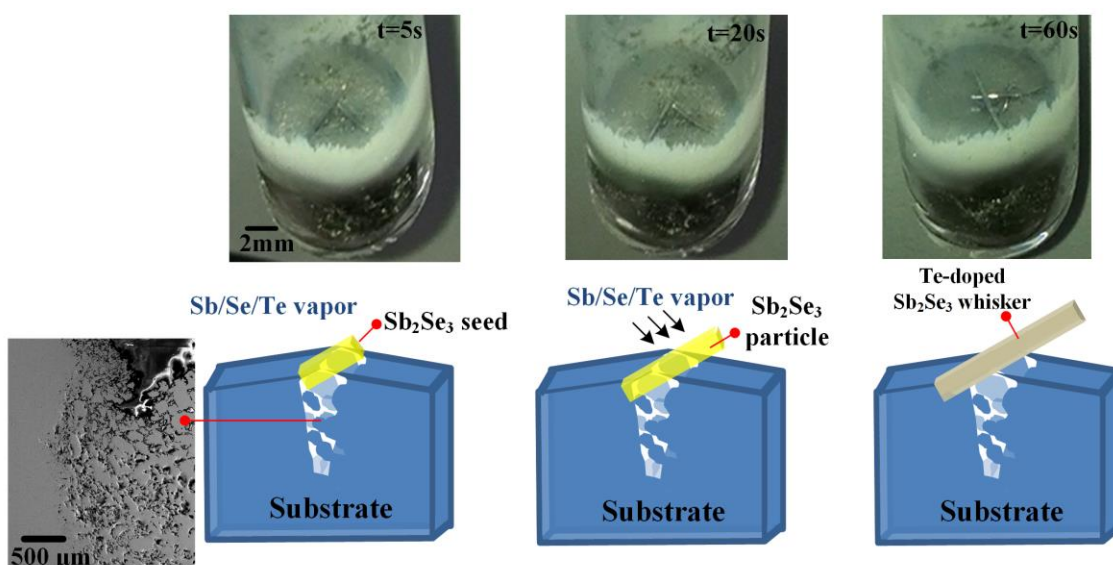


Fig. 1 Proposed Vapor-solid (VS) mechanism for the Te-doped Sb_2Se_3 whisker growth

thermopower wave resource, as both materials exhibit high Seebeck values, high electrical conductivity and high anisotropic structure¹⁶. The Sb_2Se_3 , which shares lots of common features with that of Bi_2Te_3 and Sb_2Te_3 , might be another perspective candidate for such a technology.

Various approaches to synthesize Sb_2Se_3 thin-film⁹ and one-dimensional Sb_2Se_3 with different architectures²⁵ are proposed, including vapor-liquid-solid (VLS)^{26,27}, hydrothermal^{25,28} and solvothermal²⁹ methods, yet the as-synthesized Sb_2Se_3 commonly oriented along the [001] crystallographic direction^{25,27,28} with only a few exceptions²⁷. To the best of our knowledge, the [010]-oriented Sb_2Se_3 was firstly discovered by

Farfán et al., who synthesized [010]-oriented Sb_2Se_3 nanowires through the VLS method²⁷. However, the anisotropic thermal/electronic transport property of [010]-oriented Sb_2Se_3 has not yet been reported. Herein, we synthesized high aspect ratio and belt-like Te-doped Sb_2Se_3 whisker that exhibits an unexpected preferential direction of [010] via a simple and low-cost self-assisted nucleation and vapor-solid (VS) growth approach. Moreover, the [010]-oriented Te-doped Sb_2Se_3 whiskers with featuring size of $1\text{cm} \times 200\mu\text{m}$ demonstrate promising PF value greater than 10^{-3} ($\text{Wm}^{-1}\text{K}^{-2}$) at 300K, revealing valuable potential for use in thermoelectric cooler.

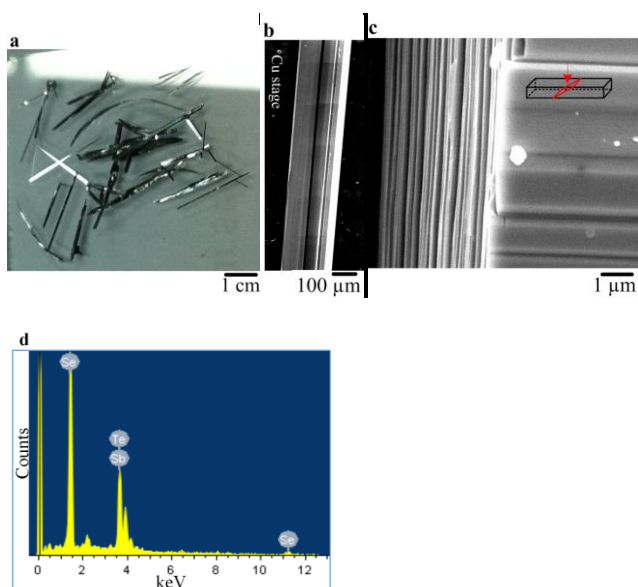


Fig. 2(a) As-grown Te-doped Sb_2Se_3 whisker. SEI (secondary electron imaging) of Te-doped Sb_2Se_3 whiskers (b) under small magnification, (c) under large magnification and tilt angle of $\theta = 30^\circ$. (d) the EDAX spectra of the Te-doped Sb_2Se_3 whiskers.

2. Results and Discussion

In this study, large scale Sb_2Se_3 whiskers were prepared through a catalyst-free and vapor-solid (VS) growth method. The proposed growth mechanism together with pictures took as the

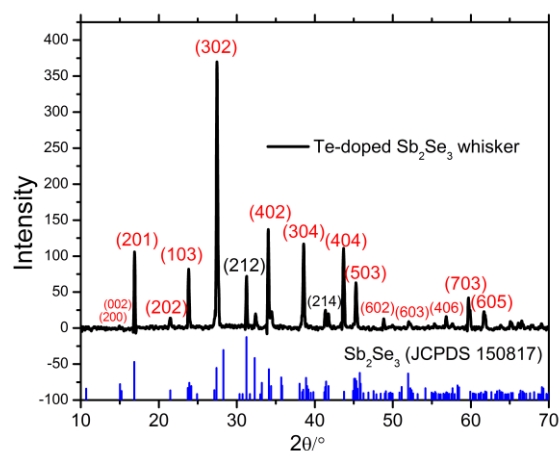


Fig. 3 XRD pattern of the Te-doped Sb_2Se_3 whisker. All the peaks are well-indexed to the orthorhombic Sb_2Se_3 (JCPDS Card No. 15-0817).

whiskers grew and a cross-sectional SEI (secondary electron imaging) image of substrate is shown in fig. 1. A porous region, resulting from solidification cracking, can be found near the centre of top surface of the substrate, and it might serve as a nucleation site that effectively induces Se and Te vapour to form Te-doped Sb_2Se_3 nuclei at an early stage of crystal growth. Formation of Sb_2Se_3 crystals with averaging size of 5mm in length is found to be completed within several tens of seconds. Fig. 2(a) and Fig. 2(b) present the morphology of the as-grown Sb_2Se_3 under small and large magnifications while fig. 2(c) shows the cross sectional area of the Sb_2Se_3 whisker with a tilt angle of 30° . Based on the cross section and plan views in fig. 2(b) and fig. 2(c), the as-grown belt-like Sb_2Se_3 is likely to result in a nanoscale-multilayers pile-up. Compositional analysis upon the whisker conducted using an energy dispersive spectrometer(EDS) is shown in figure 2(d) and reveals an average value of 61.3at%Se-37.6at%Sb-1.1at%Te despite the varying x in starting compositions of the substrates ($\text{Sb}_{37.5}\text{Se}_{62.5-x}\text{Te}_x$), indicating that the doping concentration of Te in Sb_2Se_3 might has a saturated value of 1 at%.

For the purposes of phase and crystallographic-orientation identifications, the techniques of x-ray diffraction (XRD) and transmission electron microscope (TEM) were employed. Fig. 3 shows the x-ray diffraction pattern of the as-grown whisker together with a standard Sb_2Se_3 pattern taken from the JCPDS database (No. 150817). The characteristic peaks of the whisker are well-indexed to an orthorhombic structure, confirming that the whisker is of Sb_2Se_3 phase. Moreover, the $(h0l)$ planes of the whisker are abnormally enhanced, such as (201), (103), (302), etc., revealing that the whisker exhibits a preferred orientation of [010].

Figs. 4(a)-(c) are the results of TEM analysis and provide more insights into the preferred orientation of the whisker. The bright-field image in small magnification (fig. 4(a)) indicates that the Sb_2Se_3 whisker exhibits high phase purity and no obvious secondary phase is present. Fig. 4(b) shows the selected area electronic diffraction (SAED) pattern, suggesting a single crystalline pattern with zone axis of [010]. Both SAED and XRD patterns conclude that the preferred

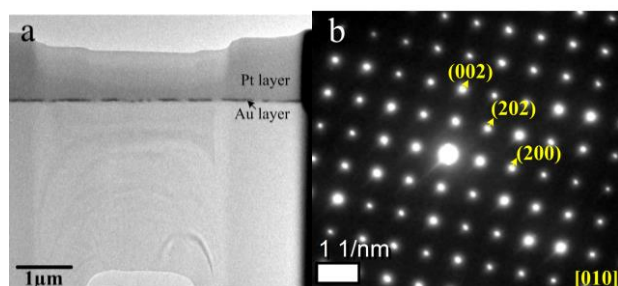


Fig. 4 TEM analysis of the Te-doped Sb_2Se_3 whisker. (a) A low-magnification TEM bright field (BF) image. (b) The electronic diffraction pattern (ED) reveals a single crystalline pattern with zone axis of [010].

orientation of the Sb_2Se_3 whisker is along [010]. The high-resolution TEM image in fig. 4(c) demonstrates the lattice structure of Sb_2Se_3 along the crystallographic direction of [010], with measured interplanar spacing $d_{002}=0.56$ nm and $d_{200}=0.58$ nm, respectively. As mentioned above, the [010]-oriented Sb_2Se_3 whisker is rarely

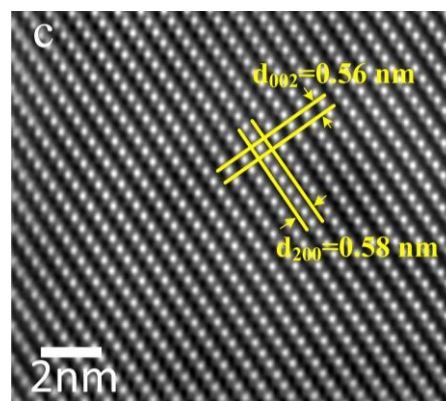


Fig. 4(c) The HRTEM image taken from the Te-doped Sb_2Se_3 whisker shows a zone axis of [010].

reported²⁷, making the whisker grown in this present work worth studying to realize the impact of preferred orientation upon the transport property and to evaluate the potential of [010]-oriented Sb_2Se_3 for applications as a thermoelectric material.

The thermoelectric property of the [010]-oriented Te-doped Sb_2Se_3 whisker is measured using the longitudinal DC steady-state method similar to that revealed in³⁰ except for thermal conductivity measurement. Given that the Sb_2Se_3 exhibits an orthorhombic structure, and the electrodeposited Sb_2Se_3 on a templet, as suggesting in³⁰ for thermal conductivity measurement, is likely to have a preferential orientation of [001] instead of [010]. Therefore, the thermal conductivity of the [010]-oriented Te-doped Sb_2Se_3 could not be simply obtained; herein, only the Seebeck coefficient and electrical resistivity within the temperature range of 300K-400K are reported. To date these transport properties (ie., Seebeck coefficient and electrical resistivity) of the [010]-oriented Sb_2Se_3 whisker is firstly discovered and will be compared with that of Sb_2Se_3 in multiple scales.

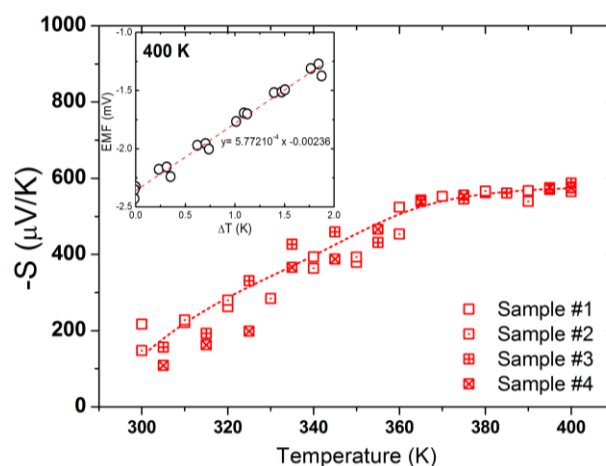


Fig. 5 (a) Seebeck coefficients of the Te-doped Sb_2Se_3 whiskers measured within 300K-400K, revealing an n type conduction. Samples #1 to #4 denote Te-doped Sb_2Se_3 whiskers obtained from the very same batch.

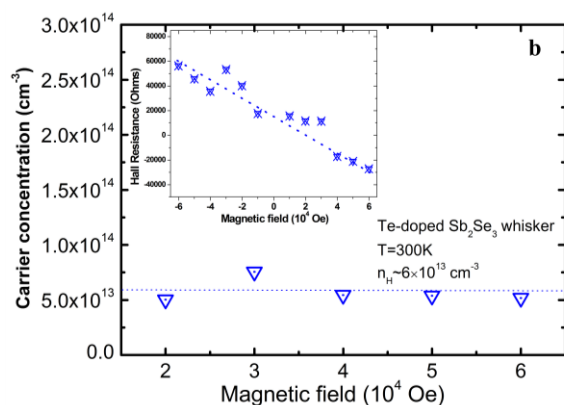


Fig. 5(b) Hall carrier concentration (n_H) of the Te-doped Sb_2Se_3 whisker measured at 300K under a magnetic field of +6T to -6T. The small inset shows the relationship between Hall resistance versus the varying magnetic field.

Fig. 5(a) presents the temperature dependent Seebeck coefficient of the Te-doped Sb_2Se_3 whiskers synthesized from the same batch. Within temperature window of 300K-400K, the Seebeck values of those whiskers generally follow a similar pattern, retaining negative values (ie., n -type material) within temperature region of 300K to 400K. At 300K, the Te-doped Sb_2Se_3 whiskers exhibits a promising Seebeck value of ~ -145 ($\mu V/K$); the Seebeck coefficient gradually increases with temperature and reaches a plateau value of -600 ($\mu V/K$) at 400K, which is comparable to the value of -750 ($\mu V/K$) obtained reported in sulfurized Sb_2Se_3 nanocrystals¹⁴. Given that the decrease in carrier concentration essentially leads to the increase in the Seebeck coefficient¹⁸ under an assumption that the effective mass remains unchanged within 300K-400K, the transport property of the Te-doped Sb_2Se_3 whisker follows a metallic-like behaviour. It should be noted that the image embedded in the upper-left corner of Fig. 5(a) represents the relation between the applied temperature differences (ΔT) across the whisker versus the obtained voltage drops (ΔV) while the slope in that image is therefore referred as the Seebeck coefficient. A nearly perfect linear relationship between the applied temperature

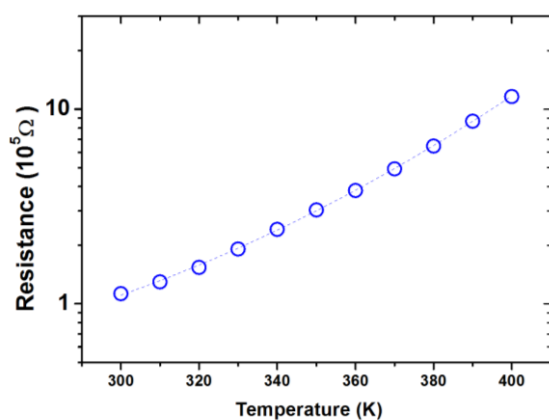


Fig. 5 (c) Electrical resistivity of the Te-doped Sb_2Se_3 whiskers measured within 300K-400K, showing the metallic-like behaviour.

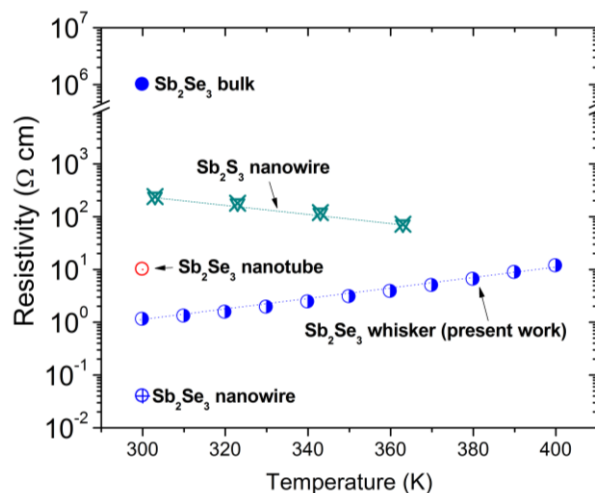


Fig. 5 (d) Electrical resistivity of the Te-doped Sb_2Se_3 whisker measured within 300K-400K, compared with that of the Sb_2Se_3 bulk^{22,23}, the Sb_2Se_3 nanowire³⁴, the Sb_2Se_3 nanotube¹⁴ and Sb_2Se_3 nanowire¹⁴, respectively.

differences (ΔT) and the obtained voltage drops (ΔV) confirms the accuracy in measurement. To the best of our knowledge, this work presents a first attempt to measure and address the temperature dependent Seebeck coefficients (thermopower) of the Sb_2Se_3 within the temperature range of 300K-400K, and the information shall be essential in developing the Sb_2Se_3 in the applications of thermoelectric cooler.

Fig. 5(b) presents the Hall carrier concentration (n_H) of the Te-doped Sb_2Se_3 whisker measured at 300K under a magnetic field of +6T to -6T using the Quantum Design physical properties measurement system (PPMS). The carrier concentration of the whisker, collecting under varying magnetic fields, appears to be a consistent value of 6×10^{13} (cm^{-3}). The small inset in Fig. 5(b) shows a nearly linear relationship between the Hall resistance *versus* varying magnetic fields (+6T to -6T); small variations can be found, presumably due to the high electrical resistance originated from sample itself and the contacts. The value of carrier concentration of the whisker (6×10^{13} (cm^{-3})) is much lower than that of optimal range (10^{19} - 10^{21} (cm^{-3})), indicating that further engineering of the carrier concentration may enhance the thermoelectric performance.

Bulk single crystal Sb_2Se_3 has been reported to exhibit high resistance of 10^6 - 10^9 (Ω) at ambient condition^{22,23,31}. While the high Seebeck value obtained from the [010]-oriented Te-doped Sb_2Se_3 also implies high electrical resistivity. The electrical measurements upon the samples with high electrical resistivity, such as insulators, might fall beyond the capability of the four-probe technique that normally used to measure the electrical resistivity of metals or semiconductors³². Nevertheless, it was found that the contact resistance in two-probe measurement gradually becomes insignificant at elevated temperature compared with the intrinsic resistance of measured segment as the diameters of wires increase³³. Therefore, the electrical resistance and resistivity of individual Sb_2Se_3 whisker measured by two-probe technique in this

study could be generally valid as the contribution of conduct resistance to the total resistance is small and negligible.

Fig. 5(c) shows the temperature-dependent electrical resistance of the individual Te-doped Sb_2Se_3 whisker measured within 300K-400K, and the values fall in a range of $10^5(\Omega)$ - $10^6(\Omega)$, which is similar to that reported in Sb_2Se_3 nanotube ($10^5(\Omega)^{14}$). The temperature-dependent resistance (Fig. 5(c)), showing a similar behaviour as that observed in the Seebeck values, increases from $10^5(\Omega)$ at 300K to $10^6(\Omega)$ at 400K and yields the corresponding electrical resistivity (ρ) of 10 - $10^2(\Omega\text{cm})$ as shown in fig. 5(d). In fig. 5(d), the electrical resistivity of [001]-oriented Sb_2S_3 nanowire³⁴, which also belongs to the family of V_2VI_3 , presents together with that of Sb_2Se_3 in various scales, including the Sb_2Se_3 nanowire¹⁴, the Sb_2Se_3 nanotube¹⁴, the Sb_2Se_3 whisker (this present work) and the Sb_2Se_3 bulk²²⁻²⁴, to gain more insights upon the electrical transport properties of layered-chalcogenide materials. In general, the [010]-oriented Sb_2Se_3 whisker demonstrates metallic-like electrical transport property and shows improved electrical conductivity among the layered-chalcogenide materials, exhibiting 10^5 and 10^1 times lower electrical resistivity than that of Sb_2Se_3 bulk materials²²⁻²⁴ and Sb_2S_3 nanowire³⁴ at room temperature, respectively. Moreover, the electrical resistivity of the Sb_2Se_3 whisker is comparable to that of Sb_2Se_3 nanotube, but still higher than that of Sb_2Se_3 nanowire¹⁴.

Fig. 5(e) summaries the temperature dependent power factor (PF , S^2/ρ) of the n -type layered-chalcogenide Sb_2Se_3 ^{14,22-24} in forms of bulk and nanostructures, which are denoted by different blue triangles. The PF of the Te-doped Sb_2Se_3 whisker, denoting by half-filled triangle, gives a promising value of $\sim 2(\mu\text{W}/\text{mK}^2)$ at 300K, increases to a peak value of $\sim 7(\mu\text{W}/\text{mK}^2)$ at 350K, and drops with increasing temperature to a value of $\sim 3(\mu\text{W}/\text{mK}^2)$ at 400K. In short, the PF value of the Te-doped Sb_2Se_3 whisker at 300K, which is of $PF \sim 2(\mu\text{W}/\text{mK}^2)$, falls slightly lower than that of Sb_2Se_3 nanowire ($PF = 56.5(\mu\text{W}/\text{mK}^2)^{14}$), locates in a similar range with that of Sb_2Se_3 nanotube ($PF = 5.6(\mu\text{W}/\text{mK}^2)^{14}$) and shows 10^4 times higher than that of Sb_2Se_3 bulk materials ($PF = 3.2 \times 10^{-4}(\mu\text{W}/\text{mK}^2)^{22-24}$), suggesting that the [010]-oriented Te-doped Sb_2Se_3 whisker exhibits enhanced thermoelectric performance compared with its bulk form, presumably resulting from remarkable improvement in the electrical conductivity.

3. Conclusions

In summary, the Te-doped Sb_2Se_3 whisker with feature size of centimetre in length and several hundreds of micrometer in width is synthesized through a self-assisted vapour-solid (VS) method, further revealing a layered structure stacked up by nano-sized sheets. Crystallographic-identification of the Sb_2Se_3 whisker, using techniques of XRD and TEM, confirms that it adopts the orthorhombic structure; nevertheless, the whisker grows along an abnormal preferred-orientation of [010], which is rarely discovered for layered-chalcogenide V_2VI_3 materials. The transport property of the [010]-oriented Sb_2Se_3 whisker, i.e., the electrical resistivity and Seebeck coefficient, are measured within 300K-400K, and further comparing with that of n -type Sb_2Se_3 materials in multi-scale forms. The power factor (PF) of Sb_2Se_3 whisker, showing a promising value of $\sim 2(\mu\text{W}/\text{mK}^2)$ at 300K, is 10^4 times higher than that of Sb_2Se_3 bulk

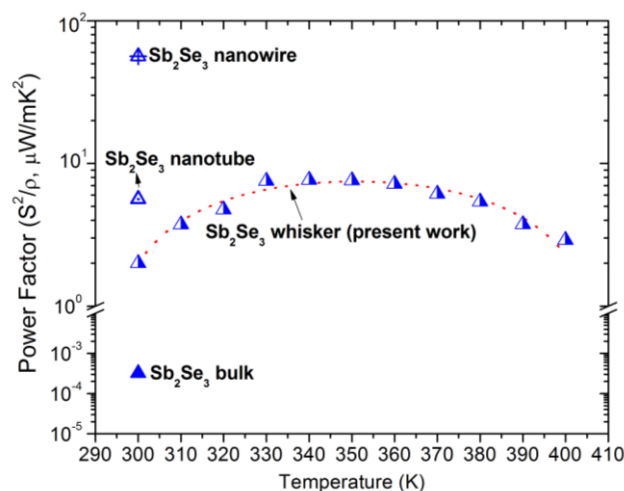


Fig. 5(e) Power factor ($S^2\rho$) of the Te-doped Sb_2Se_3 whisker (the present work) within 300K-400K. Comparisons of power factors between the Sb_2Se_3 whisker (the present work), the Sb_2Se_3 nanowire¹⁴, the Sb_2Se_3 nanotube¹⁴, the Sb_2Se_3 bulk^{22,23} are shown. The dotted curves are drawn to guide the eyes.

material. This might result from great enhancement in electrical conductivity and high Seebeck coefficient of the [010]-oriented Sb_2Se_3 whisker, implying that the Sb_2Se_3 whisker with preferential orientation holds enormous possibility for application in thermoelectric cooling device.

4. Experimental Section

4.1 Te-doped Sb_2Se_3 whisker preparation.

Ingots of 5g were prepared using the pure elements of Te (99.99 wt.%, Aldrich, USA), Se(99.99 wt.%, Aldrich, USA) and Sb(99.999 wt.%, Sigma-Aldrich, USA). The pure elements that weighed according to the proportion of $\text{Sb}_{37.5}\text{Se}_{62.5-x}\text{Te}_x$ ($x=1.25, 2.5, 3.75, 5$ and 6.25) were homogenized under vacuum at 1073K for 6 hours and subsequently quenched in water. The ingot was ground into powder, loaded in a 10×12 mm quartz tube, and melted under vacuum again from room-temperature to 1073K with a constant heating rate of 50K/hr. After homogenizing at 1073K for 2 hours, the ampoule was slowly cooled down from 1073K to 523K with a cooling rate 50K/hr, and immediately removed from the furnace. The whiskers could be collected from the top of the ingot and subjected for further analysis and measurement.

4.2 Characterization.

The as-grown whisker was further glued on Cu-stage for metallographic observation and compositional analysis using a scanning electron microscope (SEM, Carl Zeiss LEO 1550VP) and an energy dispersive spectrometer (EDS, Oxford 6587, England), respectively. Phase identification of the whisker was conducted by using a powder x-ray diffractometer (Philips X-Pert Pro; Cu $K\alpha$ radiation) with a Cu $K\alpha$ target, at angles (2θ) of 20 - 90° . The obtained diffraction pattern was further compared with the JCPDS database (Joint Committee on Powder Diffraction Standard). A

transmission electronic microscope (TEM, JEOL 2100HT, LaB6), equipped with EDS, was used to gain more sights on the crystal structure and preferential orientation of the whisker. Bright-field image, high-resolution image and selected-area diffraction pattern were obtained by using the TEM analysis. A focused ion beam (FIB, FEI Nova 200, Japan) was employed for TEM sample preparation, using Ga⁺ ion as a source to thin the sample. The ion-thinning sample with thickness less than 100nm was then placed on carbon coated copper/gold mesh using a glass probe, and subjected to TEM analysis.

4.3 Thermoelectric property.

Longitudinal DC steady-state method³⁰ was applied to measure the Seebeck coefficient of Sb₂Se₃ whiskers in temperature range 300 to 400 K. At given temperature, an electrical resistance heater was driven by programmable power supply to create a small temperature gradient across the sample. The generated temperature gradient (ΔT), and the thermal EMF (ΔV) were monitored by two pairs of T-type differential thermocouple. Typically, ΔT is set in the range of 0.5-1 K, and a statistically averaged $S = -\Delta V / \Delta T$ value was derived from the slope of a ΔV vs ΔT plot as shown in the inset of fig. 5. The detail of the measurement procedure was also described in³⁰. Hall measurement was performed in the Quantum Design physical properties measurement system (PPMS, Quantum Design) at 300K and the Hall coefficient R_H was obtained using the Van der Pauw technique under a reversible magnetic field of 6 T.

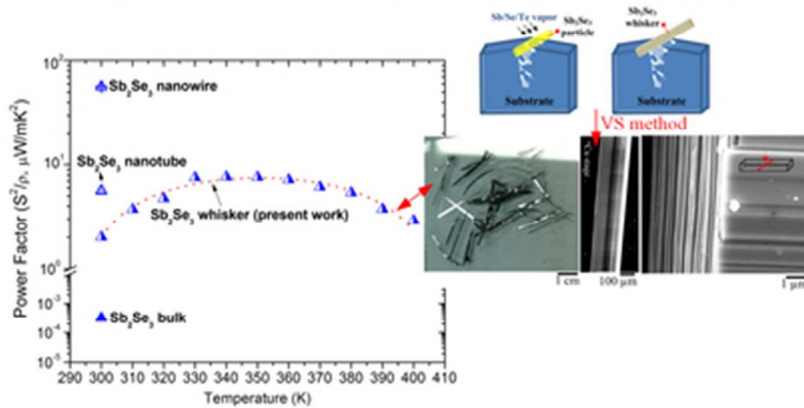
Acknowledgements

The authors acknowledge the financial support of Ministry of Science and Technology of Taiwan (MOST 103-2218-E-110-007-MY2).

References

- L. D. Hicks and M. S. Dresselhaus, *Phys. Rev. B*, 1993, 47, 16631-16634.
- Y. M. Lin, X. Z. Sun, and M. S. Dresselhaus, *Phys. Rev. B*, 2000, 62, 4610-4623.
- N. Mingo. *Appl. Phys. Lett.*, 2004, 84, 2652-2654.
- L. D. Zhao, S. H. Lo, Y. Zhang, H. Sun, G. Tan, C. Uher, C. Wolverton, V. P. Dravid and M. G. Kanatzidis. *Nature*, 2014, 508, 373-377.
- I. Efthimiopoulos, J. Zhang, M. Kucway, C. Park, R. C. Ewing and Y. Wang. *Sci. Rep.*, 2013, 3, 2665.
- B. R. Chakraborty, B. Ray, R. Bhattacharya and A.K. Dutta. *J. Phys. Chem. Solids*, 1980, 41, 913-917.
- H. W. Chang, B. Sarkar and C. W. Liu. *Crystal Growth & Design*, 2007, 7, 2691-2695.
- S. Sun, Y. Xing and R. Jin. *J. Nanosci. Nanotechnol.*, 2013, 13, 5910-5913.
- M. Z. Xue and Z. W. Fu, *J. Alloys Compd.*, 2008, 458, 351-356.
- S. Messina, M.T.S. Nair and P.K. Nair. *J. Electrochem. Soc.*, 2009, 156, H327-H332.
- A.M. Fernandez and M.G. Merino. *Thin Solid Films*, 2000, 366, 202-206.
- P. Pramanik and R.N. Bhattacharya. *Phys. Status Solidi A*, 1972, 13(1), K1.
- H. Nili, S. Walia, S. Balendhran, D. B Strukov, M. Bhaskaran and S. Sriram. *Adv. Funct. Mater.*, 2014, 24, 6741-6750.
- R. J. Mehta, C. Karthik, W. Jiang, B. Singh, Y. Shi, R. W. Siegel, T. Borca-Tasciuc and G. Ramanath. *Nano Lett.*, 2010, 10, 4417-4422.
- W. Choi, S. Hong, J. T. Abrahamson, J.-H. Han, C. Song, N. Nair, S. Baik and M. S. Strano. *Nature Mater.*, 2010, 9, 423-429.
- S. Walia, R. Weber, S. Sriram, M. Bhaskaran, K. Latham, S. Zhuiykov and K. Kalantar-zadeha. *Energy Environ. Sci.*, 2011, 4, 3558-3564.
- S. Shimizu, W. Choi, J. T. Abrahamson and M. S. Strano. *Phys. Status Solidi.*, 2011, 248, 2445-2448.
- G. J. Snyder and E. S. Toberer. *Nature Mater.*, 2008, 7, 105-114.
- Y.L. Chen, J.G. Analytis, J.H. Chu, Z.K. Liu, S.K. Mo, X.L. Qi, H.J. Zhang, D.H. Lu, X. Dai, Z. Fang, S.C. Zhang, I.R. Fisher, Z. Hussain, Z.X. Shen. *Science*. 2009, 325, 178-181.
- L. E. Bell. *Science*. 2008, 321, 1457-1461.
- M.G. Kanatzidis. *Chem. Mater.*, 2010, 22, 648-659.
- L. G. Gribnyak and T. B. Ivanova. *Inorg. Mater.*, 1987, 23, 478-482.
- B. R. Chakraborty, B. Ray, R. Bhattacharya and A. K. Dutta. *J. Phys. Chem. Solids*, 1980, 41, 913-917.
- X. W. Zheng, Y. Xie, L.Y. Zhu, X.C. Jiang, Y.B. Jia, W.H. Song, Y.P. Sun. *Inorg. Chem.*, 2002, 41, 455-461.
- X. Yan, B. Poudel, Y. Ma, W. S. Liu, G. Joshi, H. Wang, Y. Lan, D. Wang, G. Chen and Z. F. Ren. *Nano Lett.*, 2010, 10, 3373-3378.
- R. B. Yang, J. Bachmann, E. Pippel, A. Berger, J. Woltersdorf, U. Gösele, and K. Nielsch. *Adv. Mater.*, 2009, 21, 3170-3174.
- W. Farfán, E. Mosquera, R. Vadapoo, S. Krishnan and C. Marin. *J. Nanosci. Nanotechnol.*, 2010, 10, 1-4.
- D. Wang, C. Song, X. Fu and X. Li. *J. Crystal Growth*, 2005, 281, 611-615.
- J. Ma, Y. Wang, Y. Wang, P. Peng, J. Lian, X. Duan, Z. Liu, X. Liu, Q. Chen, T. Kim, G. Yao and W. Zheng. *Cryst. Eng. Comm.*, 2011, 13, 2369-2374.
- C.L. Chen, Y. Y. Chen, S. J. Lin, J. C. Ho, P. C. Lee, C.D. Chen and S. R. Harutyunyan. *J. Phys. Chem. C*, 2010, 114, 3385-3389.
- P. P. Kong, F. Sun, L. Y. Xing, J. Zhu, S. J. Zhang, W. M. Li, Q. Q. Liu, X. C. Wang, S. M. Feng, X. H. Yu, J. L. Zhu, R. C. Yu, W. G. Yang, G. Y. Shen, Y. S. Zhao, R. Ahuja, H. K. Mao and C. Q. Jin. *Sci. Rep.*, 2014, 4, 6679.
- A.G. MacDiarmid, W.E. Jones, I.D. Norris, J. Gao, A.T. Johnson, N.J. Pinto, J. Hone, B. Han, F.K. Ko, H. Okuzaki and M. Llaguno. *Synth. Metals*. 2001, 119, 27-30.
- Y. Ze Long, J. L. Duvail, M. M. Li, C. Gu, Z. Liu, S. P. Ringer. *Nanoscale Res. Lett.*, 2010, 5, 237-242.
- H. Bao, X. Cui, C. M. Li, Q. Song and Zhisong Lu and J. Guo. *J. Phys. Chem. C*, 2007, 111, 17131-17135.

The thermoelectric power factor of the self-assisted [010]-oriented Sb_2Se_3 is 10^4 times higher than that of Sb_2Se_3 bulk and is comparable to that of Sb_2Se_3 nanotube, respectively



39x19mm (300 x 300 DPI)